

Ground effects in time-domain simulations of outdoor sound propagation

Didier Dragna (1), Philippe Blanc-Benon (1) and Franck Poisson (2)

(1) Laboratoire de Mécanique des Fluides et d'Acoustique, UMR CNRS 5509, École Centrale de Lyon, 69134 Écully Cedex, France

(2) SNCF, Direction de l'Innovation et de la Recherche, 75379 Paris Cedex 08, France

PACS: 43.28.Js, 43.28.En, 43.20.El

ABSTRACT

Finite difference time-domain (FDTD) methods are accurate and efficient methods to solve the linearized Euler equations that governed long range sound propagation. Interactions between pressure fluctuations and local wind and temperature profile as well as a complex topography are readily taken into account. The main issue in time-domain methods is to account for reflection of acoustic waves on an impedance ground. Impedance boundary conditions are classically defined in frequency-domain and cannot be directly translated in time-domain. Thus, a time-domain boundary condition (TDBC) has been recently proposed by Cotté *et al.* (1) for applications in outdoor sound propagation. This TDBC has been implemented in a FDTD solver using several methods developed in the community of computational aeroacoustics. In this paper, propagation of an initial gaussian pulse is considered in a two-dimensional geometry over a distance of 500 m with a frequency resolution up to 1200 Hz. The results are compared in time-domain with an analytical solution. The waveforms of the acoustic pressure are found to be strongly dependant on the impedance model. Surface waves are also identified in the numerical calculations.

INTRODUCTION

Outdoor sound propagation is governed by many complex phenomena which can be ordered in two groups: on one hand, atmospheric effects due mainly to refracting induced by vertical profile of wind and temperature, atmospheric absorption and scattering by turbulent structures and on the other hand boundary effects due to ground impedance and topography. Moreover, for applications in transportation noise, acoustic sources are also complex: in the case of the TGV - the french high-speed train - they are broadband and in motion (320 km/h). Time-domain numerical solutions of the linearized Euler equations can account precisely for all these phenomena (2, 3) and are becoming increasingly popular (2, 4–6). Modelling of impedance grounds is one of the main difficulties in time-domain solvers since the impedance models are defined in the frequency-domain. Several methods have been proposed in the literature: some authors choose to model the ground layer in their computational domain (4) while others have developed time-domain impedance boundary condition (TDBC). In this paper, the TDBC recently proposed by Cotté *et al.* (1) for applications in outdoor sound propagation is implemented.

This paper aims at studying propagation of acoustics waves from an initial gaussian pulse over an impedance ground and over a distance of 500 m. Three impedance models classically used for applications in outdoor sound propagation are considered. The major contribution at the ground level for two impedance models is a low-frequency wave. Comparison with an analytical solution shows that this wave corresponds to the surface wave.

TIME-DOMAIN SIMULATIONS

Solver description

The linearized Euler equations (LEEs) are solved by using explicit numerical schemes developed by the community of computational aeroacoustics. Optimized finite-difference schemes and selective filters over 11 points are used for spatial derivation and for grid-to-grid oscillations removal, respectively. For the interior points, fourth-order finite-difference scheme of Bøgey and Bailly (7) and six-order selective filters are applied. For boundary points, non-centered schemes are used. The filtering coefficient is set to 0.2 for all filters except at the extreme points where a filtering coefficient of 0.01 is applied. At last, time integration uses the linear six-step fourth-order Runge Kutta algorithm of Berland *et al.* (8). At the ground, the TDBC developed by Cotté *et al.* (1) is used. At the other boundaries, a radiation boundary condition is applied.

The domain of interest has a length of 500 m in the x -direction and of 50 m in the z -direction. An uniform spatial step $\Delta x = \Delta z = 0.05$ m is used in both directions. The computational domain has then 22 millions of points. The Courant-Friedrich-Levy number denoted as CFL and defined by $CFL = c_0 \Delta t / \Delta x$ is set to 1 where $c_0 = 340$ m/s is the adiabatic sound speed. 11 000 time iterations are needed so that the pressure pulse leaves the computational domain. An homogeneous atmosphere is considered and the air density ρ_0 is set to 1.22 kg/m^3 .

Source

In the simulation, an initial gaussian pulse is considered:

$$p(x, z, t = 0) = S_0 \exp\left(-\ln 2 \frac{x^2 + (z - z_S)^2}{B_x^2}\right) \quad (1)$$

where z_S is the height of the source, S_0 is a parameter set to 1 Pa and $B_x = 5\Delta x$ is the gaussian halfwidth. In this paper, the acoustic pressure is normalized by the parameter S_0 .

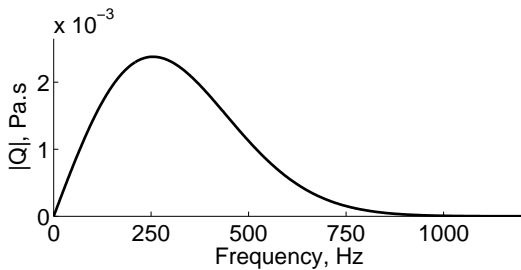


Figure 1: Amplitude of the equivalent point source strength versus frequency.

This source can be seen as a monopole with an equivalent source strength $Q(\omega)$. Indeed, the analytical solution of propagation of this pulse in free field can be written as the product of the Green function times a parameter denoted as $Q(\omega)$ that depends only on frequency. This term is given by:

$$Q(\omega) = S_0 \frac{\pi B^2}{c_0} i k_0 \exp\left(-\frac{k_0^2 B^2}{4}\right) \quad (2)$$

where ω is the angular frequency, k_0 is the acoustic wavenumber and the parameter B is linked to B_x by the relation $B^2 = B_x^2 / \ln 2$. On figure 1, the absolute value of $Q(\omega)$ is plotted versus frequency. It can be seen that this source has frequency components up to 800 Hz (-30 dB compared to the maximum value of $|Q(\omega)|$). In the numerical simulations, the source is located at $x = 0$ and its height is set to $z_S = 2$ m.

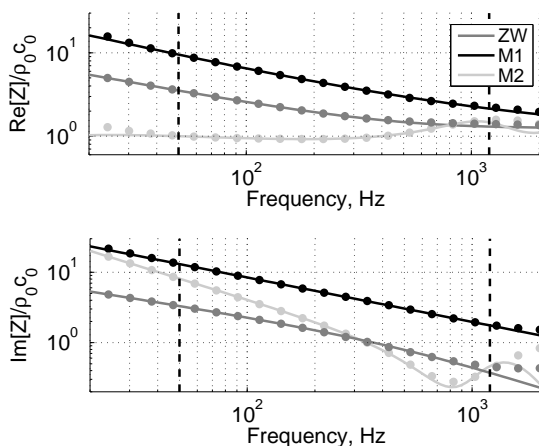


Figure 2: Real and imaginary parts of the normalized impedance models (in full lines) and of their approximations (in dots). The two vertical lines delimit the frequency band on which the optimization process has been realized.

Impedance model

Impedance models $Z(\omega)$ are usually defined in the frequency-domain by the relation :

$$P(\omega) = Z(\omega) V_n(\omega), \quad (3)$$

where $V_n(\omega)$ and $P(\omega)$ represent respectively the component of acoustic velocity normal to the ground and the pressure at the interface between the ground and the air. To translate directly the impedance boundary condition in time-domain, a convolution that is not efficient numerically is then needed. To avoid this calculation, following work done in electromagnetic propagation (9) and applied in acoustics for duct configurations (10), a method proposed by Cotté *et al.* (1) for applications in outdoor sound propagation is used. First, the impedance model is approximated in the frequency-domain by a rational function:

$$Z(\omega) \approx \sum_{k=0}^N \frac{A_k}{\lambda_k - i\omega} \quad (4)$$

where the parameters λ_k and A_k are respectively the poles of the model and corresponding coefficients and N is the number of poles. A recursive convolution method, numerically efficient, can then be used. Several methods are available to get the approximation of the impedance model and are described in Cotté *et al.* (1). Three impedance models are considered here:

- the modified Zwickler and Kosten impedance model (11):

$$Z_{ZK} = Z_\infty \left(1 + \frac{\mu_{ZK}}{-i\omega}\right)^{1/2} \quad (5)$$

with $Z_\infty = \frac{\rho_0 c_0 q}{\Omega}$ and $\mu_{ZK} = \frac{\sigma_0 \Omega}{\rho_0 q^2 \gamma}$. This model depends on the tortuosity q , the porosity Ω and the flow resistivity σ_0 . We choose here the following set of coefficients for the impedance model, denoted as ZW: $q=1$, $\Omega = 0.8$ et $\sigma_0 = 10$ kPa.s.m⁻². This model can represent an semi-infinite snowy ground.

- the Miki impedance model (12) :

$$Z_M = \rho_0 c_0 \left(1 + \frac{\mu}{(-i\omega)^{0.632}}\right), \quad (6)$$

with $\mu = 0.1279(2\pi\sigma_e)^{0.632}$. This model has only one parameter, the effective flow resistivity σ_e . We use here $\sigma_e = 100$ kPa.s.m⁻² which is a common value for grassy grounds. This model will be denoted as M1.

- the two-parameter Miki impedance model (12, 13) :

$$Z_{Me} = Z_M \coth \left[\frac{e}{c_0} (-i\omega + \mu_e (-i\omega)^{0.382}) \right], \quad (7)$$

with $\mu_e = 0.193(2\pi\sigma_e)^{0.618}$. The parameter e is called the equivalent thickness of the porous layer. The set of coefficients $e = 0.1$ m and $\sigma_e = 10$ kPa.s.m⁻² is chosen and can model a rigidly backed layer of thickness e and of impedance Z_M . This model will be referred as M2.

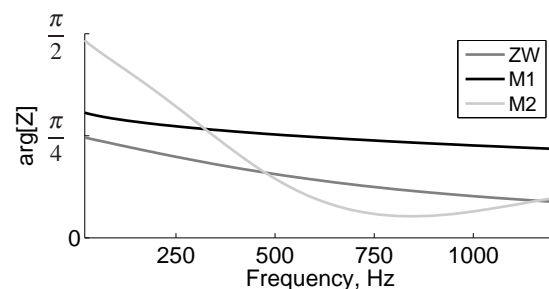


Figure 3: Phase of the three impedance models versus frequency.

The coefficients of the approximation in equation 4 are calculated with a method of optimization in the frequency-domain on the frequency band [50 Hz ; 1200 Hz] with $N = 5$. The real and the imaginary parts of the impedance models and of their approximations are plotted on figure 2. It can be seen that a good approximation has been obtained through the frequency band of interest.

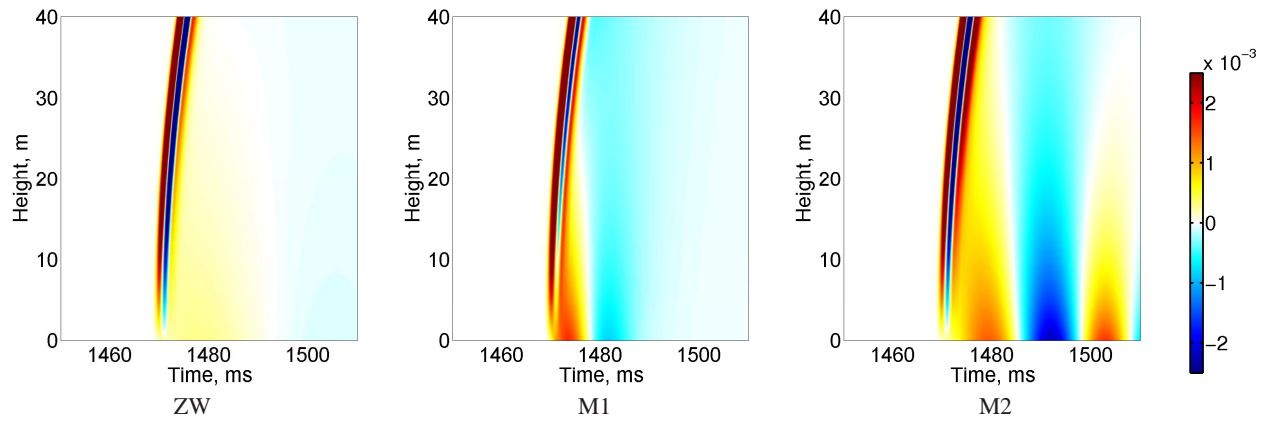


Figure 4: Waveforms of the normalized pressure obtained for the three different impedance models at a column of receivers located at $x = 500$ m from the source. On the right, the colorbar scale indicates the normalized pressure.

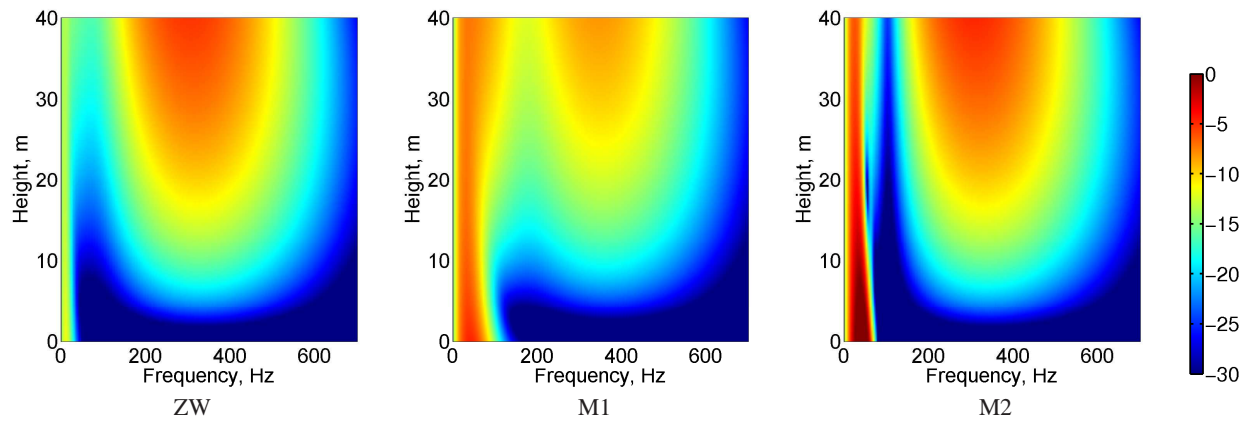


Figure 5: Sound pressure levels in dB obtained for the three different impedance models at a column of receivers located at $x = 500$ m from the source. On the right, the colorbar scale indicates the sound pressure level in dB.

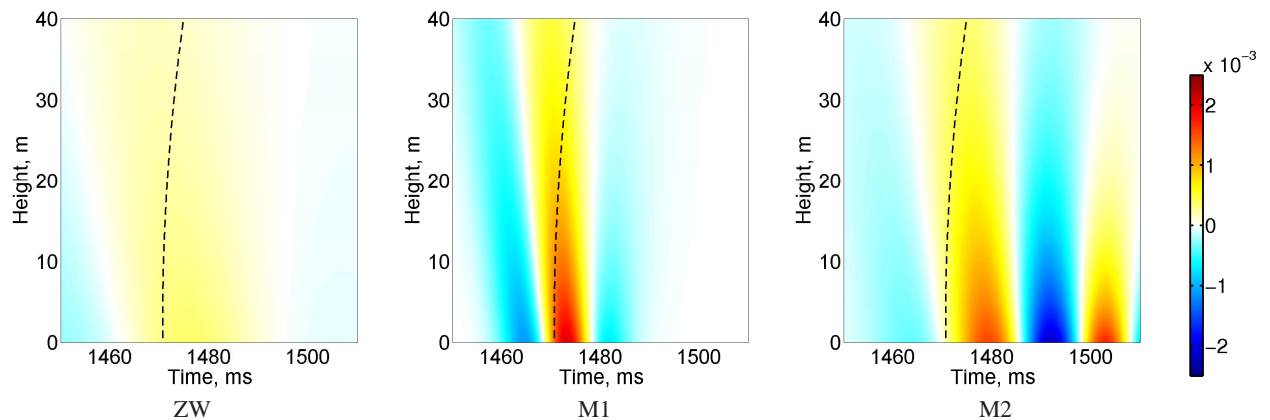


Figure 6: Waveforms of the surface wave obtained from the analytical solution for the three different impedance models at a column of receivers located at $x = 500$ m from the source. The dotted lines represent the arrival time of the direct wave. On the right, the colorbar scale indicates the normalized pressure.

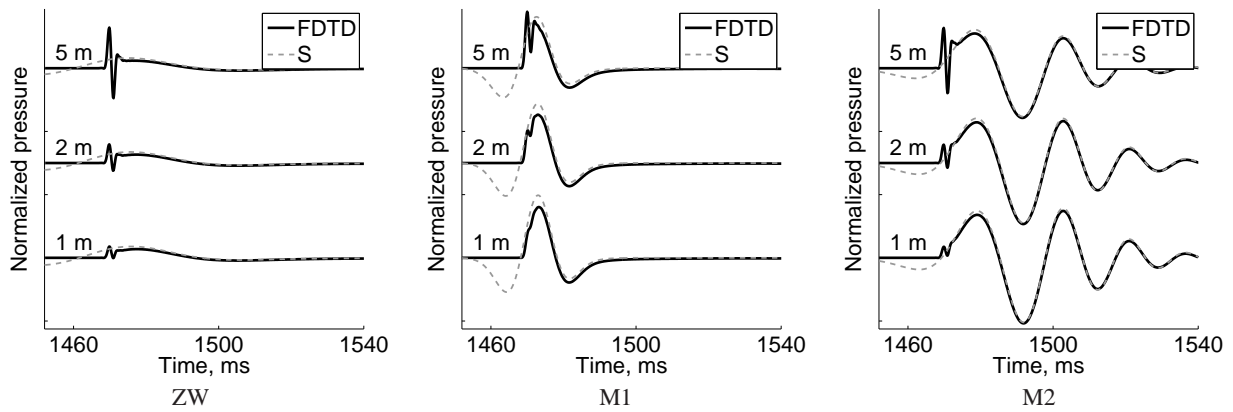


Figure 7: Comparison between the waveforms obtained from numerical calculations (in full line) and the waveform of the surface wave obtained with an analytical solution (in dotted line) for the different impedance models at three receivers at different heights.

At last, the phase of the impedance models are plotted versus the frequency on figure 3. This parameter is related to the relative contribution of the surface wave: indeed, amplitude of the surface wave compared to the amplitude of total field seems more important for large values of the phase (14). For impedance models with both real and imaginary parts positive, the phase ranges from 0 to $\pi/2$. It can be noticed that the model ZW has the lower phase values for frequencies below 300 Hz. At the opposite, the phase of the M2 reach values close to $\pi/2$ for low frequencies.

RESULTS

Waveforms

The pressure waveforms $p(t)$ obtained for a column of receivers located at $x = 500$ m and at height from 0 m to 40 m are plotted on figure 4 for the three impedance models. Firstly, it can be seen that the first arrival corresponds to the direct wave in the three cases. A second arrival can be distinguished and corresponds to the reflected wave on the ground. This wave depends strongly on the impedance model. The waveforms for receivers close to the ground are notably different: the waveform duration of these arrivals is much longer to those of the direct and the reflected waves. Thus, a quasi-harmonical behavior can be noticed, especially for the case of the model M2 where the decay of oscillations with time is small.

On figure 5, the sound pressure level ΔL defined by $\Delta L = 20 \log(\hat{p}/\hat{p}_{ref})$ is plotted versus frequency. The reference pressure is set to $\hat{p}_{ref} = 2.10^{-5}$ Pa. Large contribution from low-frequencies can be seen on the spectra for receivers close to the ground in the three cases; the frequency band and the amplitude of this contribution depend on the impedance model. Thus, for the model ZW, frequency components of pressure are neglectable for frequency above 30 Hz while this limit is close to 100 Hz for the model M1. Moreover, amplitude of this low-frequency contribution is greater for the model M2 than for the model M1. Thereafter, it will be shown that this contribution correspond to the surface wave.

Surface wave

The surface wave is a distinct contribution propagating above an impedance plane. Among its properties, it should be noticed that this wave decay exponentially with height. In the 3D case, it decays with the square root of range while the direct and the reflected waves decay linearly with range. At long ranges, surface waves can then become the major contribution to acoustic pressure.

An interesting interpretation has been proposed by Waxler (15) : in the theory of modal expansions, the surface wave corresponds to the first mode. The analytical expression for the surface wave can then be obtained in a two-dimensional configuration for a monopole source of unit amplitude assuming an homogeneous atmosphere. The following equation is then proposed:

$$\hat{p}_S(x, z, \omega) = \frac{k_S}{\sqrt{k_0^2 - k_S^2}} e^{i\sqrt{k_0^2 - k_S^2}x} e^{-ik_S(z+z_S)}, \quad (8)$$

where $k_S = k_0\beta$ is the vertical wavenumber of the surface wave and $\beta = \rho_0 c_0 / Z$ is the normalized admittance. The surface wave component is then given in the time-domain by:

$$p_S(x, z, t) = \frac{1}{2\pi} \int_{-\infty}^{+\infty} Q(\omega) \hat{p}_S(x, z, \omega) e^{-i\omega t} d\omega, \quad (9)$$

where the expression of $Q(\omega)$ can be found in the equation 2. A Discrete Fourier Transform is used to compute efficiently the equation 9.

The analytical waveforms of the surface wave have been represented on figure 6 for the different impedance models. Close to the ground, the waveforms observed on figure 4 are retrieved, especially the quasi-harmonical behavior. It can be also noted that the amplitude of the surface waves is larger with important values of the impedance phase at low frequencies. Thus, the large oscillations obtained with the model M2 and the low amplitude of the surface wave with the model ZW are consistent with the figure 3. Besides, it can be observed that a part of the surface wave is non-causal: indeed, in the different cases, the surface wave is non-zero before arrival of the direct wave. This means that the speed of the surface wave is greater than the sound speed. It is one of the classical features of the surface waves (16). However, in the numerical calculations, this non-causal part of the surface wave does not appear: analytical calculations could show that it is cancelled by the reflected wave.

Comparison with the analytical solution

In this section, the waveforms of the pressure obtained from the numerical calculations are compared to the waveform of the surface wave obtained from the analytical solution. On the figure 7, these two waveforms have been plotted for receivers located at $x = 500$ m and at heights of 1 m, 2 m and 5 m. It can be seen that in the different cases the surface wave component corresponds well with the tail of the signal. Note also the acausal part of the surface wave. At last, it can be noted that,

in the cases M1 and M2, the major contribution to pressure at the ground level comes from the surface wave; for the case ZW, it is less obvious because the amplitude of the surface wave is very low.

CONCLUSION

In this paper, a numerical simulation of outdoor sound propagation over a distance of 500 m has been studied. Surface waves depending on the ground impedance have been observed. It has been shown that the low-frequency tails of the pressure signal correspond to the surface waves for the different impedance models considered in this work. At last, it has been observed that the shape and the amplitude of the waveforms of the surface wave depend strongly on the impedance model. In future work, propagation of acoustic waves over terrain with a complex topography will be studied. Indeed, surface wave can also exist in acoustic shadow zones. It will be then interesting to study its contribution to the pressure and to compare its influence with the other types of acoustic waves.

ACKNOWLEDGMENTS

Support by CNRS and SNCF is gratefully acknowledged. This work was granted access to the HPC resources of IDRIS under the allocation 2010-022203 made by GENCI (Grand Equipement National de Calcul Intensif).

REFERENCES

- [1] B. Cotté, P. Blanc-Benon, C. Bogey, and F. Poisson. Time-domain impedance boundary conditions for simulations of outdoor sound propagation. *AIAA J.*, 47(10):2391–2403, 2009.
- [2] B. Cotté and P. Blanc-Benon. Time-domain simulations of sound propagation in a stratified atmosphere over an impedance ground. *J. Acoust. Soc. Am.*, 125(5):EL 202–207, 2009.
- [3] D. Dragna, P. Blanc-Benon, and F. Poisson. Effects of topography in time-domain simulations of outdoor sound propagation. In *Sixteenth AIAA/CEAS Aeroacoustics Conference, Stockholm, Sweden*, 2010. AIAA Paper 2010-3758.
- [4] E.M. Salomons, R. Blumrich, and D. Heimann. Eulerian time-domain model for sound propagation over a finite-impedance ground surface. comparison with frequency-domain models. *Acta Acustica united with Acustica*, 88:483–492, 2002.
- [5] M. Hornikx. *Numerical modelling of sound propagation to closed urban courtyards*. PhD thesis, Chalmers University of Technology, 2009.
- [6] G. Guillaume, J. Picaut, G. Dutilleux, and B. Gauvreau. Use of the transmission line matrix method for the sound propagation modelling in open-space. In *Thirteenth Long Range Sound Propagation Symposium, Lyon*, 2008. <http://www.olemiss.edu/depts/ncpa/LRSP.htm>.
- [7] C. Bogey and C. Bailly. A family of low dispersive and low dissipative explicit schemes for flow and noise computations. *J. Comp. Phys.*, 194:194–214, 2004.
- [8] J. Berland, C. Bogey, and C. Bailly. Low-dissipation and low-dispersion fourth-order runge-kutta algorithm. *Computers & Fluids*, 35:1459–1463, 2006.
- [9] R.J. Luebbers and F. Hunsberger. FDTD for nth-order dispersive media. *IEEE Trans. Antennas Propag.*, 40(11):1297–1301, 1992.
- [10] Y. Reymen, M. Baelmans, and W. Desmet. Time-domain impedance formulation suited for broadband simulations. In *Thirteenth AIAA/CEAS Aeroacoustics Conference, Rome, Italy*, 2007. AIAA Paper 2007-3519.
- [11] V.E. Ostashev, S.L. Collier, D.K. Wilson, D.F. Aldridge,

- N.P. Symons, and D.H. Marlin. Padé approximation in time-domain boundary conditions of porous surfaces. *J. Acoust. Soc. Am.*, 122(1):107–112, 2007.
- [12] Y. Miki. Acoustical properties of porous materials - modifications of delany-bazley models. *J. Acoust. Soc. Jpn.*, 11(1):19–24, 1990.
- [13] K.B. Rasmussen. Sound propagation over grass covered ground. *J. Sound. Vib.*, 78(2):247–255, 1981.
- [14] J.E. Piercy, T.F.W. Embleton, and L.C. Sutherland. Review of noise propagation in the atmosphere. *J. Acoust. Soc. Am.*, 61(6):1403–1418, 1977.
- [15] R. Waxler, K.E. Gilbert, and C. Talmadge. A theoretical treatment of the long range propagation of impulsive signals under strongly ducted nocturnal conditions. *J. Acoust. Soc. Am.*, 124(5):2742–2754, 2008.
- [16] D.G. Albert. Observations of acoustic surface waves in outdoor sound propagation. *J. Acoust. Soc. Am.*, 113(5):2495–2500, 2003.